引用格式:CHEN Yang, GAO Ming, HU Xue-lei, *et al*. Design of Co-aperture Wide Spectrum Compound Eye Optical System [J]. *Acta Photonica Sinica*, 2020, **49**(3):0322002
陈阳,高明,胡雪蕾,等. 共口径宽光谱复眼光学系统设计[J].光子学报,2020,**49**(3):0322002

共口径宽光谱复眼光学系统设计

陈阳[1],高明[1],胡雪蕾[1],张玺斌[2],焦旸[3]
(1 西安工业大学 光电工程学院,西安 710021)
(2 中国科学院西安光学精密机械研究所,西安 710119)
(3 西北机电工程研究所,陕西 咸阳 712099)

摘 要:为了扩大复眼光学系统的接收光谱,研究了一种可见光、长波红外复眼光学系统.推导了双波段共焦面方程,建立了子眼系统与接收系统的匹配要求.子眼光学系统的工作波段为 0.38~0.78 μm 和8~12 μm,焦距为 5 mm,相对孔径为 1∶3,视场为 10°.两个波段的子眼系统成像位置均为 2.92 mm,相邻的两个中心光轴夹角为 4.016°,共 650 个子眼,合并后的视场为 90°.接收系统的焦距为 4 mm,视场为 80°,相对孔径为 1∶3.子眼系统和接收系统的图像质量良好,在-40~60 ℃的温度范围内无热差影响.

关键词:复眼;宽光谱;共像面;光学设计;透镜阵列
中图分类号:O439 **文献标识码**:A **doi**:10.3788/gzxb20204903.0322002

Design of Co-aperture Wide Spectrum Compound Eye Optical System

CHEN Yang[1], GAO Ming[1], HU Xue-lei[1], ZHANG Xi-bin[2], JIAO Yang[3]
(1 *Institute of Optoelectronic Engineering, Xi'an Technological University, Xi'an* 710021, *China*)
(2 *Xi'an Institute of Optics and Precision Mechanics of CAS, Xi'an* 710119, *China*)
(3 *Northwest Institute of Mechanical & Electrical Engineering, Xianyang, Shaanxi* 712099, *China*)

Abstract: In order to expand the receiving spectrum of the compound eye optical system, a visible light and long wave infrared wide spectrum compound eye optical system was studied. The dual-band ommatidia common image equation was derived, and the matching requirement between ommatidia and the receiving system was established. The ommatidia optical system has working bandwidths of 0.38~0.78 μm and 8~12 μm, a focal length of 5 mm, a relative aperture of 1∶3, and a field of view of 10°. The imaging position of the ommatidia system in both the bands is 2.92 mm. The angle between two neighboring center optical axes of the neighboring ommatidia is 4.016°, with 650 ommatidia, and the combined field of view is 90°.The receiving optical system has a focal length of 4 mm, a field of view of 80° and a relative aperture of 1∶3. The ommatidia system and receiving system show good image quality, without any thermal effects in the temperature range of -40 ℃ to 60 ℃.

Key words: Compound eye; Wide spectrum; Common image; Optic design; Lens array
OCIS Codes: 140.0140; 110.0110; 170.0170; 220.0220

0 Introduction

The compound eye of insects consists of a large number of sub-eyes, each of which can form a

Foundation item: Army Equipment Preresearch Project (No. 301XXX102), Key Laboratory of Shaanxi Provincial Department of Education (No. 17JS052)
First author: CHEN Yang(1986—), male, lecturer, M.S. degree, mainly focuses on optical design. Email: 867549558@qq.com
Supervisor (Contact author): GAO Ming (1964—), male, professor, Ph.D. degree, mainly focuses on atmospheric transmission and optical design. Email: minggao1964@163.com
Received: Oct.22, 2019; **Accepted**: Dec.24, 2019

independent photosensitivity[1]. Due to the special structure of compound eye, insect compound eye has the advantages of small size[2,3], large field of view and sensitivity to moving objects[4,5]. At present, there are many researches on compound eye system on these advantages[6,7]. However, most of these researches ignore another advantage of insect compound eye-broad spectrum[8]. Studies have shown that the compound eyes of many insects have good imaging in the ultraviolet, infrared[9,10]. Wide-spectrum compound eyes are of great significance for insects to adapt to natural environment. Especially for insects that live at night or in dense forests, or other low light environments, the wide-spectrum compound eye can capture more effective information[11]. Besides, wide-spectrum also play an important role in insect foraging[12,13], flight navigation and other behaviors[14,15]. Therefore, in order to improve the complex environmental adaptability of compound eye optical system, and receive target information more effectively and comprehensively, it is necessary to design wide-spectrum compound eye optical system.

This paper proposes a wide-spectrum compound eye structure capable of receiving both visible and long-wave infrared bands, and specifically designs the ommatidia and receiving optical system. Using the focal power matching method, the imaging positions of the two bands of light passing through the ommatidia system are made identical, and the matching conditions are used to ensure that the light of the ommatidia system can enter the receiving system. The compound eye system has a wide imaging range and compact structure, which improves the capabilities of system image acquisition.

1 Principle of common path compound eye optical system

1.1 Sub-eye common image theory

In order to receive the image formed by the ommatidia, the image planes of the visible light and the long-wave infrared band are required to be at the same position. However, the refractive indices of the same material in the different wavelength bands are dissimilar, as showed in Fig 1. According to the focal power Eq. (1) of the single lens and focal power Eq.(2) of the single lens, for the same lens, the degree of deflection of each band of light is different, and the final image planes of the two bands will not be at the same position.

$$\begin{bmatrix} l & 0 \\ 0 & l' \end{bmatrix} = \begin{bmatrix} l & l' \\ f' & f' \end{bmatrix} \tag{1}$$

where l' is the image distance, l is the object distance, and f' is the focal length of the lens.

$$\begin{bmatrix} f'n & d \\ f'(1-n) & r_1 - r_2 \end{bmatrix} = \begin{bmatrix} \dfrac{n}{n-1} & 0 \\ 0 & r_1 r_2 \end{bmatrix} \tag{2}$$

where n is the refractive index, r_1, r_2 are the curvature of the two faces of the lens, and d is the lens thickness.

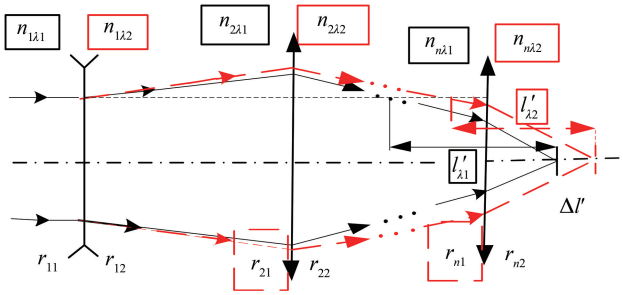

Fig.1 The difference in image plane position of the sub-eye optical system

According to the above formula, we obtain

$$\begin{bmatrix} l'n(n-1) & -r_1 r_2 \\ n & l(r_1 - r_2) \end{bmatrix} + \begin{bmatrix} l'n(n-1) & dl \\ l'(n-1) & dl \end{bmatrix} = \begin{bmatrix} r_1 r_2 & 0 \\ 0 & nl \end{bmatrix} \tag{3}$$

To image at the common positionat different bands, the imaging planes to coincide

$$\begin{cases}\begin{bmatrix}\frac{1}{l'_{\lambda1}} & 0\\ 0 & 1\end{bmatrix}=\begin{bmatrix}(r_1-r_2)n_{\lambda1} & (r_1-r_2)\\ \frac{1}{r_1r_2} & \frac{1}{r_1r_2}\end{bmatrix}+\begin{bmatrix}dn_{\lambda1} & 2d\\ \frac{1}{r_1r_2} & \frac{1}{r_1r_2}\end{bmatrix}+\begin{bmatrix}d & 1\\ \frac{1}{l} & \frac{1}{r_1r_2n_{\lambda1}}\end{bmatrix}\\ \begin{bmatrix}\frac{1}{l'_{\lambda2}} & 0\\ 0 & 1\end{bmatrix}=\begin{bmatrix}(r_1-r_2)n_{\lambda2} & (r_1-r_2)\\ \frac{1}{r_1r_2} & \frac{1}{r_1r_2}\end{bmatrix}+\begin{bmatrix}dn_{\lambda2} & 2d\\ \frac{1}{r_1r_2} & \frac{1}{r_1r_2}\end{bmatrix}+\begin{bmatrix}d & 1\\ \frac{1}{l} & \frac{1}{r_1r_2n_{\lambda2}}\end{bmatrix}\end{cases} \tag{4}$$

where $l'_{\lambda1}$, $l'_{\lambda2}$ are the image distances of the two bands, $n'_{\lambda1}$, $n'_{\lambda2}$ are the refractive indices of the two bands.

Subtracting the two parts of Eq. (4), we obtained

$$\begin{bmatrix}l'_{\lambda2} & l'_{\lambda1}\\ \frac{1}{l'_{\lambda1}l'_{\lambda2}} & \frac{1}{l'_{\lambda1}l'_{\lambda2}}\end{bmatrix}=\begin{bmatrix}r_1(n_{\lambda1}-n_{\lambda2}) & r_2(n_{\lambda1}-n_{\lambda2})\\ \frac{1}{r_1r_2} & \frac{1}{r_1r_2}\end{bmatrix}+\begin{bmatrix}d(n_{\lambda1}-n_{\lambda2}) & d\,\frac{(n_{\lambda1}-n_{\lambda2})}{n_{\lambda1}n_{\lambda2}}\\ \frac{1}{r_1r_2} & \frac{1}{r_1r_2}\end{bmatrix} \tag{5}$$

when $l'_{\lambda2}=l'_{\lambda1}-\Delta l'$, we obtained

$$\begin{bmatrix}\Delta l' & 0\\ 0 & \frac{1}{l'_{\lambda1}(l'_{\lambda1}-\Delta l')}\end{bmatrix}=\begin{bmatrix}\Delta n & \Delta n\\ \frac{1}{r_1} & \frac{1}{r_2}\end{bmatrix}+\begin{bmatrix}\Delta n & \Delta n\\ \frac{d}{r_1r_2n_{\lambda1}n_{\lambda2}} & \frac{1}{r_1r_2}\end{bmatrix} \tag{6}$$

Since $\Delta l'$ is far less than $l'_{\lambda1}$, $l'_{\lambda2}$, when $l'_{\lambda1}l'_{\lambda2}\approx l'^2_m$, $n_{\lambda1}n_{\lambda2}\approx n^2_{\lambda m}$, l'_m, $n_{\lambda m}$ are the image distance and refractive index of intermediate wavelength $\left(\lambda_m=\frac{\lambda_1+\lambda_2}{2}\right)$.

$$\begin{bmatrix}\Delta l' & 0\\ 0 & 1\end{bmatrix}\approx\begin{bmatrix}\Delta n & \Delta n\\ \frac{l'^2_m}{r_1} & \frac{l'^2_m}{r_1}\end{bmatrix}+\begin{bmatrix}\Delta n & \Delta n\\ \frac{dl'^2_m}{r_1r_2} & \frac{dl'^2_m}{r_1r_2n^2_{\lambda m}}\end{bmatrix} \tag{7}$$

It can be seen from the Eq. (7) that the imaging position inconsistency of the system in different bands is determined by the ideal imaging position, lens curvature, thickness and focal length difference of the two bands. According to Eq. (7), in order to make the single lens have the same imaging position in both bands, which should be satisfied $r_1-r_2+d=0$ and $d=0$ at the same time. At this time, the lens focal power is zero, which has no practical significance.

Considering that the actual optical system is generally composed of several lenses, and each lens produces an imaging position deviation which is different in magnitude and sign, the final image plane position can be achieved by canceling each other by different lens image plane differences. Combined with the optical system superposition theory, the total image plane position difference between the two bands is the accumulation of the image plane position difference produced by each lens, which can be expressed as

$$\begin{bmatrix}\Delta S' & 0\\ 0 & 1\end{bmatrix}=\begin{bmatrix}\Delta l'_1 & 0\\ 0 & \alpha_2\alpha_3\cdots\alpha_n\end{bmatrix}+\begin{bmatrix}\Delta l'_2 & 0\\ 0 & \alpha_3\alpha_4\cdots\alpha_n\end{bmatrix}\cdots\begin{bmatrix}\Delta l'_i & 0\\ 0 & \alpha_{i+1}\alpha_{i+2}\cdots\alpha_n\end{bmatrix} \tag{8}$$

where $\Delta S'$ is the total imaging position difference of the system in the two bands, α_i is the magnification of the difference in imaging position of the i-th lens. Considering $\Delta l'$ is the distance in the axial direction, α_i can be approximated by the intermediate wavelength axial magnification $\left(\alpha_i\approx\alpha_{im}=\frac{l'_m}{l_m}\right)$ in practical applications.

1.2 Receiving system calculation

In order to ensure that the ommatidia system and the receiving system are compatible, the object surface of the receiving system should be equal to or greater than the image plane of the ommatidia combination system. Additionally, the curvatures of the two systems need to be identical. This ensures that the images of each sub-eye system can enter the receiving system. At the same time, the aperture of the receiving system should be greater than the aperture of the edge sub-eye light, so that the light of the edge sub-eye system can enter the receiving system. Known ommatidia system aperture is D_s, the focal length is f_s, the curvature of the distribution of the ommatidia system is R, aperture is D_0, the distance from the sub-eye to the receiving system along the axis is L, the receiving system has a diameter D, and the field of view is ω, the projection aperture of the edge of the ommatidia in the vertical direction of the receiving system is ΔD, the angular magnification of the first lens of the receiving system is γ.

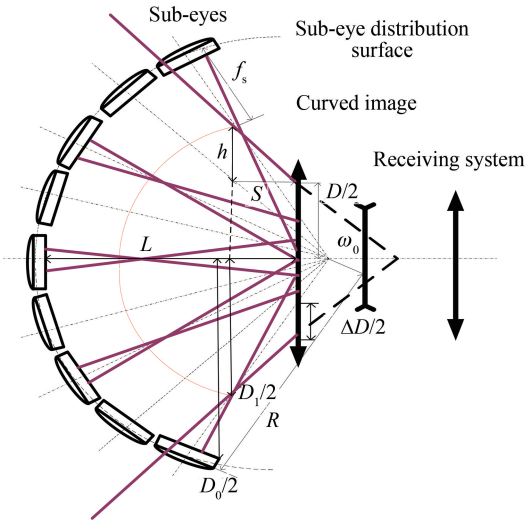

Fig.2 Matching the sub-eye and receiving optical system

Considering a single lens for the sub-eye, the distance to the image plane is approximately equal to the focal length, and the imaging surface of the sub-eye combination system should be a spherical surface. The geometric imaging principle can be used to obtain the matching formula of the sub-eye and the receiving system which is based on the aperture division structure.

$$\begin{bmatrix} \omega & 0 \\ 0 & r \end{bmatrix} = \begin{bmatrix} D_0 & 0 \\ 0 & \dfrac{1}{2} \end{bmatrix} \tag{9}$$

$$\begin{bmatrix} D & -2h \\ 1 & 1 \end{bmatrix} = \begin{bmatrix} D_0 & -\Delta D \\ 1 & \dfrac{1}{2} \end{bmatrix} \tag{10}$$

where h is the difference between the aperture of the receiving system and the curved image surface is satisfied $h = \tan\omega \cdot \gamma \cdot s$.

According to the geometric considerations, the following relationship is satisfied between the known quantity and the intermediate quantity in the formula

$$\begin{cases} \begin{bmatrix} s & 0 \\ 0 & 1 \end{bmatrix} = \begin{bmatrix} L - f_s & r_c \\ (1 - \cos\omega_0) & 1 \end{bmatrix} \\ \begin{bmatrix} \cos\omega_0 & 0 \\ 0 & 1 \end{bmatrix} = \begin{bmatrix} \sqrt{4R^2 - D_0^2} & 0 \\ 0 & \dfrac{1}{2R} \end{bmatrix} \\ \begin{bmatrix} r_c & 0 \\ 0 & 1 \end{bmatrix} = \begin{bmatrix} R & f_s \\ 1 & 1 \end{bmatrix} \\ \begin{bmatrix} D_2 & 0 \\ 0 & 1 \end{bmatrix} = \begin{bmatrix} r_c & 0 \\ 0 & \sin\omega_0 \end{bmatrix} \\ \begin{bmatrix} \Delta D & 0 \\ 0 & 1 \end{bmatrix} = \begin{bmatrix} D_s & D_s \\ 1 & \dfrac{l}{f_s} \end{bmatrix} \end{cases} \tag{11}$$

Substituting the Eq. (11) into the conditional Eqs. (9) and (10), the matching requirements for the compound-eye optical system based on the aperture division are satisfied

$$\begin{bmatrix} \omega & 0 \\ 0 & 1 \end{bmatrix} = \begin{bmatrix} D_0 & 0 \\ 0 & \dfrac{1}{2R} \end{bmatrix} \tag{12}$$

$$\begin{bmatrix} D & 0 \\ 0 & 1 \end{bmatrix} = \begin{bmatrix} 2\tan\omega \cdot \gamma & 2\tan\omega \cdot \gamma \\ R & L \end{bmatrix} + \begin{bmatrix} \sqrt{4R^2 - D_0^2} & \sqrt{4R^2 - D_0^2} \\ \dfrac{1}{2} & f_s \end{bmatrix} + \begin{bmatrix} (R - f_s)D_0 & (L - f_s)D_s \\ \dfrac{1}{f_s} & \dfrac{1}{2R} \end{bmatrix} \tag{13}$$

2 Design of optical system

2.1 Design of sub-eye

In order to verify the correctness of the above method, acommon imaging position visible and long wave infrared band wide spectrum sub-eye optical system is designed, as shown in Table 1, the focal length is $f'=5$ mm, the relative aperture is $D/f'=1/3$, and the FOV is 10°.

Table 1 The parameters of the sub-eye lens

	Visible	LWIR
Wave	0.38～0.76 μm	8～12 μm
Focal length	5 mm	
F/#	3	
Field of view	10°	
$\Delta l'$/mm	0	

The optical system consist of three-pieces lens is used as the initial structure of the dual-band sub-eye system. The wavelength of the visible light center is 0.587 μm, whereas the wavelength of the long-wave infrared is 8.2 μm. After several iterations, a two-band sub-eye initial structure with the same image plane position is obtained. The image positions of the two bands are at 3.0 mm. The parameters are shown in Table 2.

Table 2 Sub-eye lens initial structure parameter

R/mm	d/mm	G	$n_{\lambda 1}$	$n_{\lambda 2}$	Δn	l'_m	$\Delta l'_1$
2.309	0.871	BAF2	1.474	1.423	0.051	2.838	−0.345
−3.518	0.200						
−2.435	0.600	PBF2	1.766	1.668	0.102	−2.184	0.290
3.721	0.985						
3.275	0.760	CSBR	1.697	1.664	0.033	2.886	−0.140
−5.487							

The initial structure only considers the on-axis point (the FOV is 0°). The imaging process of the apposition compound eye is to mosaic a plurality of images obtained by the ommatidia to obtain a complete image with a larger FOV. The angle between the ommatidia axis and the FOV of the sub-eye is one of the important factors influencing the overall structure of the compound eye optical system. Therefore, analyzing the relationship between the FOV of the sub-eye system and the total FOV of the compound eye is the key to determining the parameters and the distribution type of sub-eye. The sub-eye lenses are equally spaced in a honeycomb arrangement. Known sub-lens lens distribution surface caliber $D_{\mathrm{LA}}=88$ mm, sub-eye lens aperture $D=2$ mm. Considering the size of the mechanical structure and the spacing between the two sub-eye lenses $d_v=4$ mm, it can be seen that the number of sub-eye lenses is

$$n=\begin{bmatrix}1 & 0\\ 0 & 1\end{bmatrix}+\begin{bmatrix}\pi & 0\\ 0 & \dfrac{1}{\tan 1/2}\end{bmatrix}+\begin{bmatrix}\pi & 0\\ 0 & \dfrac{1}{\tan 1/4}\end{bmatrix}+\cdots\begin{bmatrix}\pi & 0\\ 0 & \dfrac{1}{\tan 1/2i}\end{bmatrix} \tag{14}$$

where $i=1,2,3\cdots$ and $i\leqslant\left[\dfrac{2D_{\mathrm{LA}}-D_m}{2D_m}\right]$, the number of sub-eye lenses calculated by the Eq. (14) is 650.

Since the distribution is equally spaced, the angle between two neighboring ommatidia is not equal, and its size is

$$\begin{bmatrix}\Delta\theta_i & 0\\ 0 & 1\end{bmatrix}=\begin{bmatrix}\arctan\dfrac{2(i+1)D_m}{R} & 0\\ 0 & \arctan\dfrac{2iD_m}{R}\end{bmatrix} \tag{15}$$

Considering the material properties and design requirements, the system uses BaF2/PBF2/CSBR

materials that can transmit both visible and medium-wave infrared light. To improve image quality, a diffractive surface is introduced on the fourth surface of the system. The designed sub-eye optical system can now receive both visible light and infrared light. Through the common image surface design, the imaging positions of visible light and long-wave infrared are both at 2.92 mm. System volume is 2 mm×5 mm, which is comparable to the single-band ommatidia system. The use of the dual-band sub-eye system can obtain more comprehensive target information, which is beneficial towards the improvement of the detection and recognition ability of the compound eye system. The final sub-eye lens structure is shown in Fig. 3.

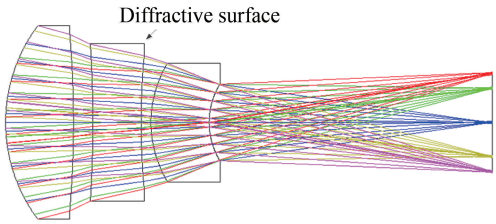

Fig.3 Sub-eye structure diagram

The designed dual-band sub-eye system parameters and diffraction surface coefficient are shown in Table 3 and Table 4.

Table 3 Dual-band sub-eye system parameters

Surf: type	Radius/mm	Thickness/mm	Glass
Standard	1.73	0.70	BAF2
Standard	−11.49	0.20	
Standard	−13.09	0.50	PBF2
Binary 2	15.28	0.10	
Standard	1.24	0.60	CSBR
Standard	0.80	2.9218	

Table 4 Diffractive surface coefficient of sub-eye

Surf: type	Surface	Norm radius	2nd coefficient	4th coefficient	8th coefficient
Binary 2	4	1	−14.386 3	−2.623 8	2.040 3

Fig.4 shows the Modulation Transfer Function (MTF) curve of the optical system under different fields of view. It can be seen that the system MTF value is greater than 0.5 at the Nyquist frequency 50 lp/mm of the visible light band, and the system MTF value can reach 0.4 at Nyquist frequency 17 lp/mm of the infrared band and the imaging quality can approach the diffraction limit.

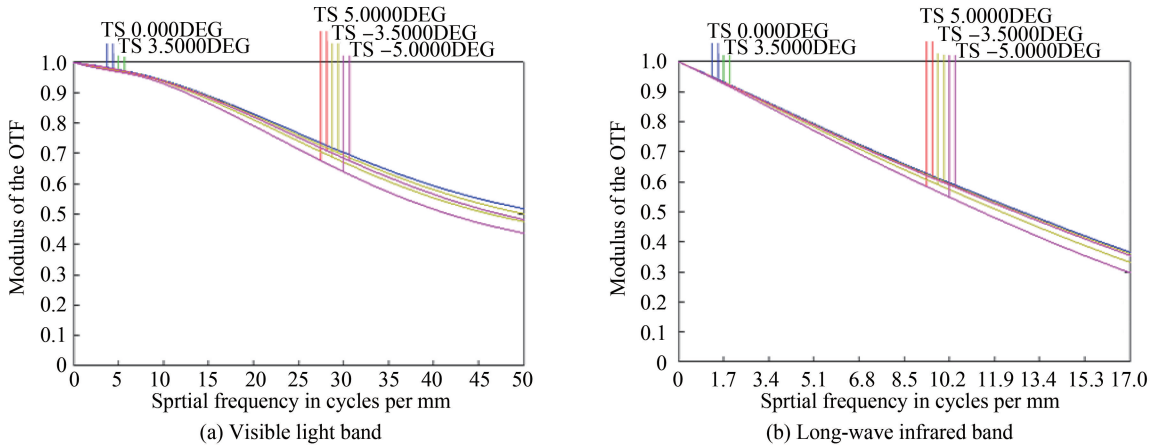

Fig.4 Sub-eye lens transfer function

Fig. 5 shows a spot diagram of the overall system. It can be seen that the RMS at the visible light band is less than 9.38 μm, and the RMS value is no more than 13.27 μm in the mid-infrared band, which are all less than one pixel size (25 μm), thereby satisfying the matching requirements of the system and the detector.

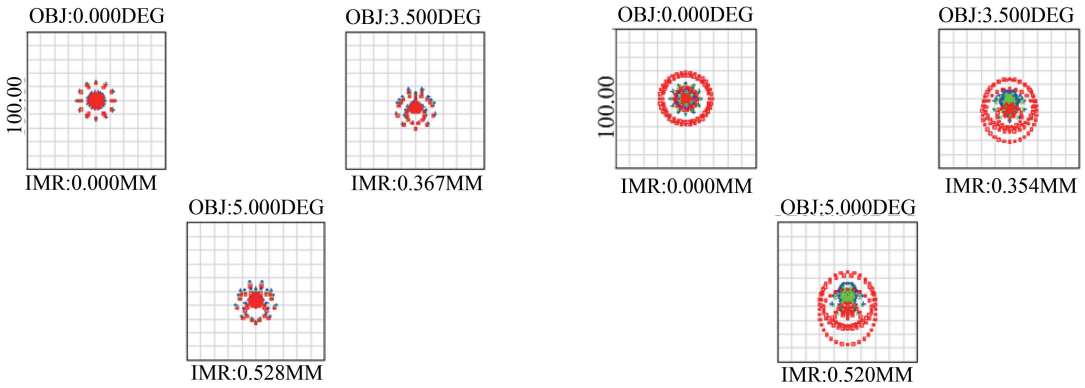

Fig.5 Sub-lens spot diagram

2.2 Design of receiving system

The receiving system has a surface curvature of 50 mm and a diameter of 80 mm. According to Eq. (13), the FOV of the receiving system is determined to be greater than 80°, and the aperture is not less than 16 mm. The specific parameters of the acceptance system are shown in Table 5.

Table 5 Receiving system technical parameters

Visible	LWIR	
Wave	0.38～0.76 μm	8～12 μm
Focal length	4 mm	
Field of view	80°	
$F/\#$	3	
Pixel	1 024×768	256×256
Pixel size	3.5 μm×3.5 μm	25 μm×25 μm

In order to reduce the system volume while ensuring the consistency of the received images in the visible and infrared bands, the receiving optical system adopts a partial common aperture structure. The final design of the receiving system has a focal length of 4 mm, a relative aperture of 1∶3 and an FOV of 80°. Synthetic FOV is $2\omega_c = 2\omega_r + 2\omega = 90°$. The receiving system consists of five lenses, three for the common part, one for the visible and one for the infrared band, with a total length of 31 mm. In order to enhance the image quality, a diffractive surface is used on the third lens. The structure of the receiving system is shown in Fig. 6. The structural parameters of the receiving optical system is listed in Table 6.

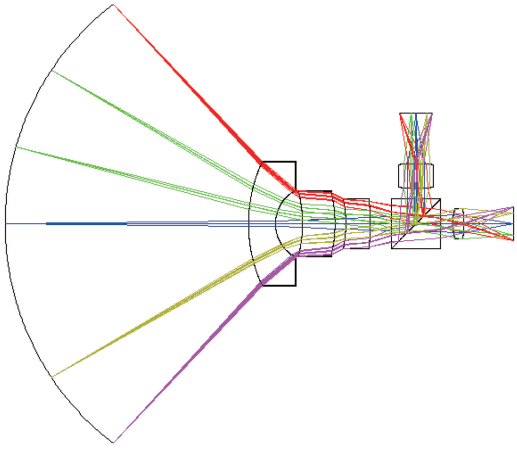

Fig.6 Receiving system structure

The parameters of the dual band receiving system are shown in Table 6. The diffraction surface coefficient is shown in Table 7.

Table 6 Dual-band compound eye receiving system parameter

	Surf:type	Radius/mm	Thickness/mm	Glass
Co-pathlens	Standard	26.40	5.00	CAF2
	Standard	6.88	5.00	
	Standard	−22.83	6.00	ZNS_BROAD
	Standard	−23.82	2.00	
	Standard	−22.96	4.50	ZNS_BROAD
	Binary 2	−41.18	3.90	
		Infinity	4.50	ZNS_BROAD
		Infinity	4.50	
		Infinity	2.29	
Visible lens	Standard	8.83	2.09	BEO
	Standard	−14.07	9.11	
		Infinity	2.00	
LWIR lens	Binary 2	−40.60	4.40	GERMANIUM
	Standard	50.89	9.24	

Table 7 Diffractive surface coefficient of receive system

Surf: type	Surface	Norm radius	2nd coefficient	4th coefficient	8th coefficient
Binary 2	6	2.5	32.02	−9.81	2.98
	9	3	−19.00	0.23	0.42

Fig.7 shows the MTF curve of the optical system in different fields of view. It can be seen that the system MTF value is greater than 0.4 at the Nyquist frequency 150 lp/mm at the visible light band and the system MTF can reach 0.4 at the Nyquist frequency 17 lp/mm at the mid-infrared band. The imaging quality here also is close to the diffraction limit.

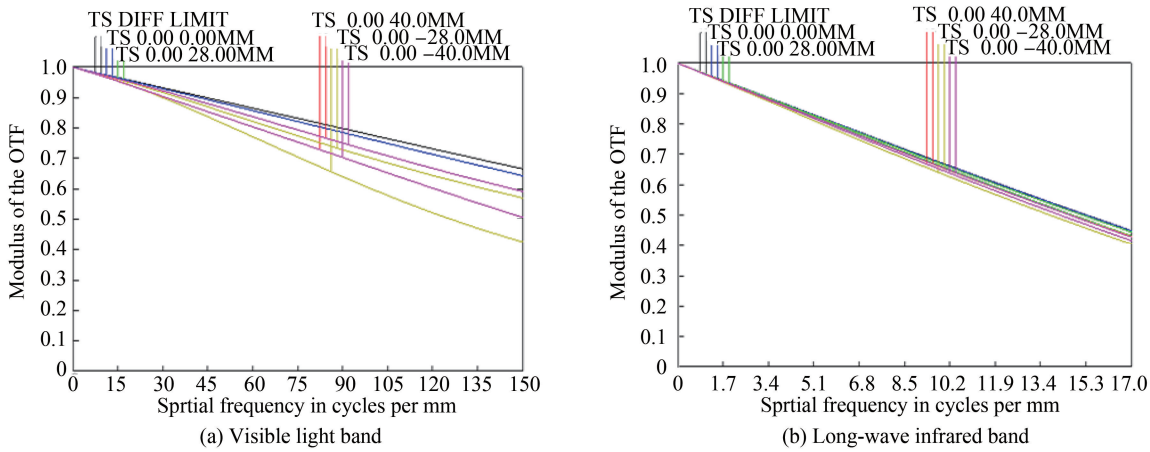

Fig.7 Receive system transfer function

Fig.8 shows a spot diagram of the overall system, where the RMS value of the visible light band is less than 2.47 μm, and the RMS value of the mid-infrared band is at most 13.82 μm, which are all in a pixel (25 μm). It satisfies the matching requirements of the system and the detector.

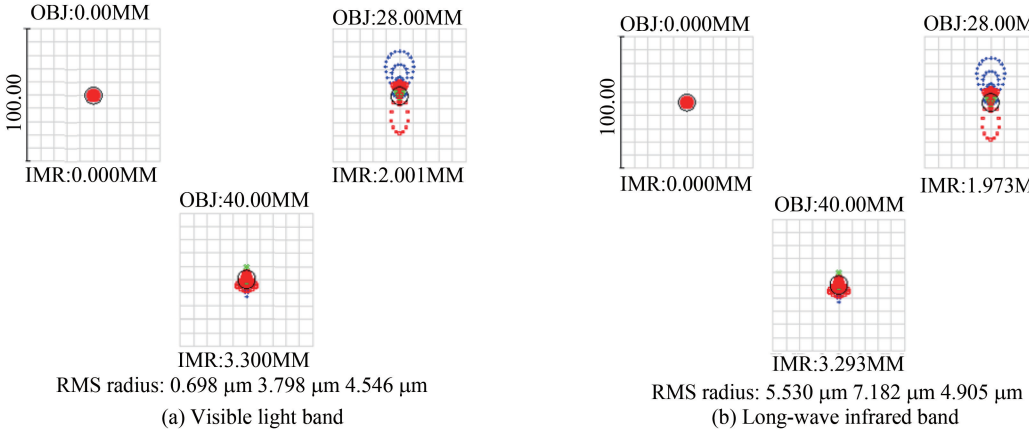

Fig.8 Receiving system spot diagram

The field of view of X-direction and Y-direction of the compound eye system are 110° and 90° respectively. Systematic sub-eyes are distributed in hexagonal shape, with a total of 650 sub-eyes. The overall picture of compound eye system and sub-eye distribution are shown in Fig. 9.

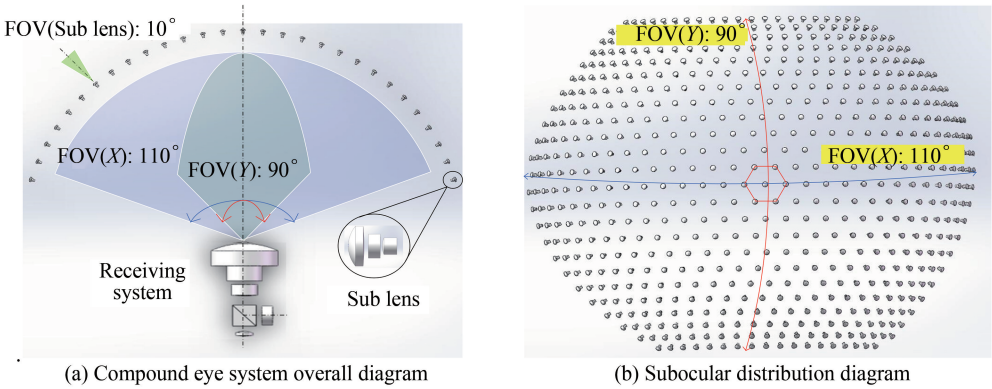

Fig.9 Compound eye system diagram

3 Athermalization and analysis

3.1 Wide spectrum athermalization

Since the system contains both visible and infrared bands, it is challenging to design the system without heating effects. It is proposed to adopt the optical passive athermalization method, in order to suppress heating by mutual compensation between materials. Fig. 10 and Fig. 13 show the MTF

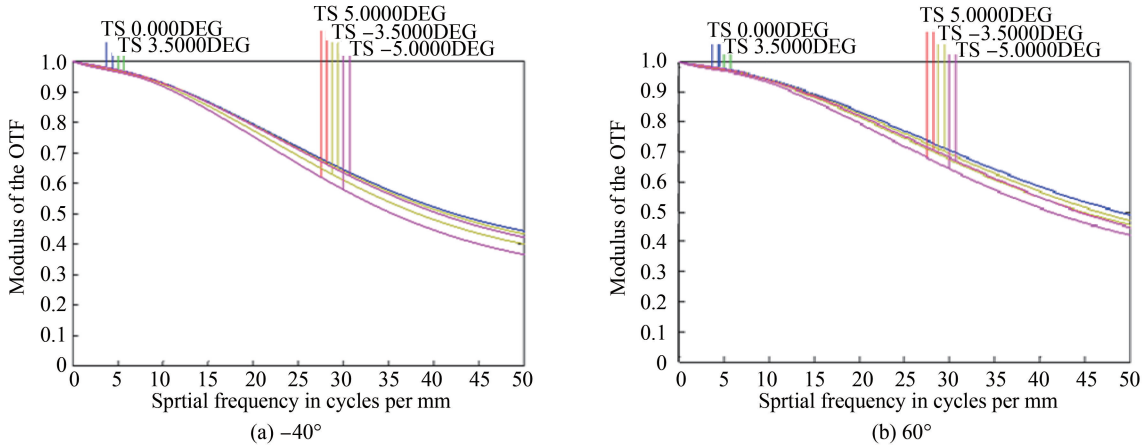

Fig.10 Visible light transfer function of the sub-eye lens

diagram of the chronograph system in the visible and long-wave infrared in the temperature range of −40 ℃ and +60 ℃. The value of the MTF is greater than 0.2 at the both visible and long-wave infrared band, which still meets the requirements of general infrared system imaging.

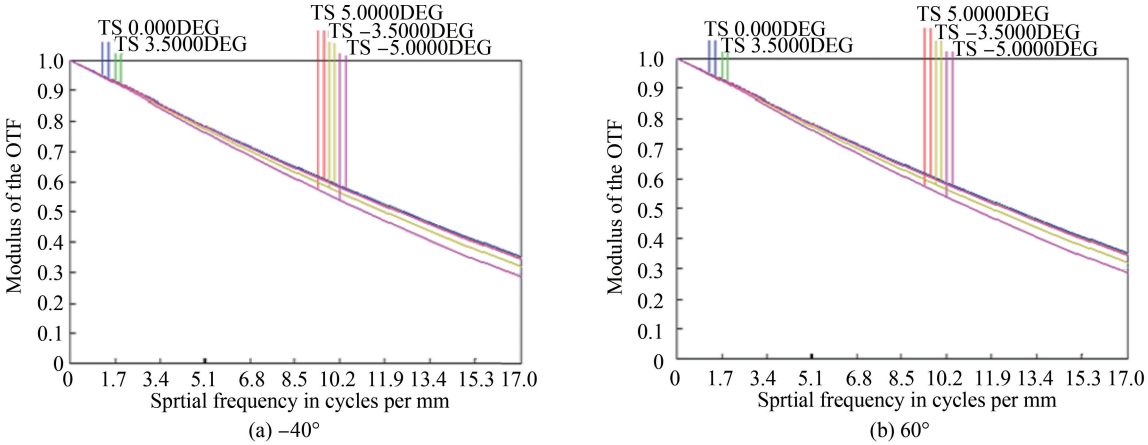

Fig.11 Long-wave infrared transfer function of the sub-eye lens

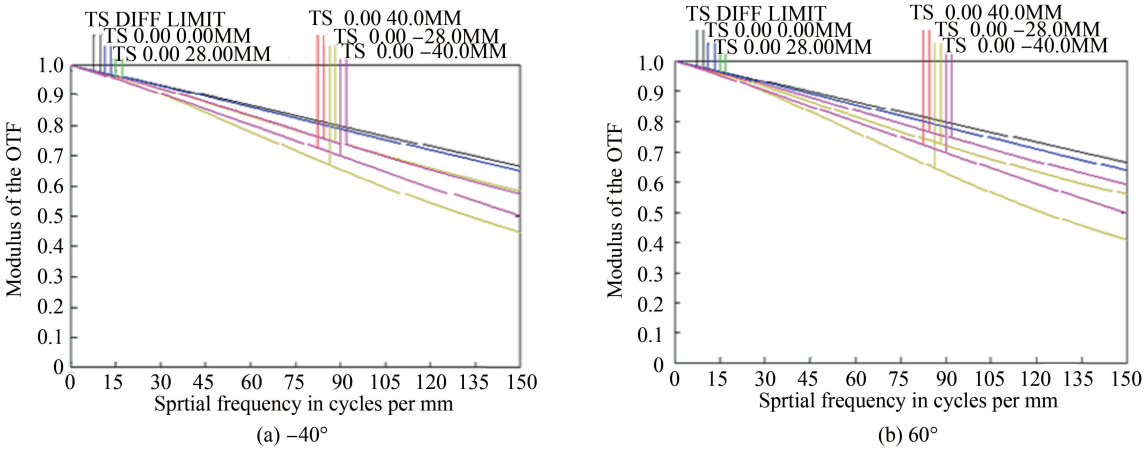

Fig.12 Visible light transfer function of receiver system

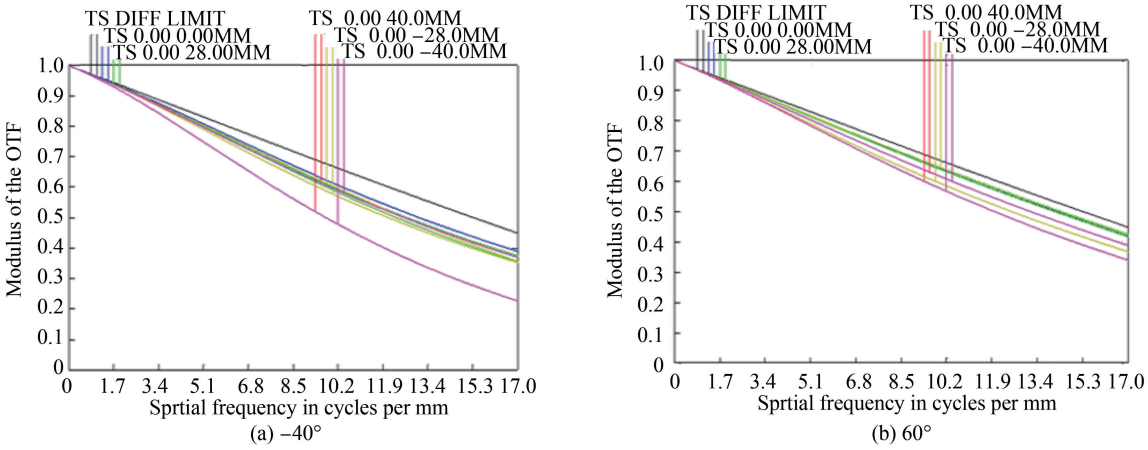

Fig.13 Infrared transfer function of the receiving system

3.2 Image plane distribution analysis

In order to reduce the difficulty of image fusion, the images of different sub-eye lenses should be separated. That is, the image height of the single sub-eye lens at the receiving system $2y'_s$ should be less than the spacing between the two sub-eye images d_s. Analysis of the designed compound eye system,

known sub-lens field of view $2\omega=10°$, the focal length $f_s=5$ mm, sub-eye synthetic surface caliber $D_c=80$ mm, Curvature $r_c=50$ mm, receiving system image height $2y'=6$ mm. From geometric optics, the image height of a single sub-eye in the receiving system is given by

$$\begin{bmatrix} y'_s & 0 \\ 0 & 1 \end{bmatrix}=\begin{bmatrix} \tan\omega \cdot f_s & 0 \\ 0 & \dfrac{2y'}{D_c} \end{bmatrix} \tag{16}$$

According to the Eq.(16), it can be calculated that $y'_s=0.078$ mm.

The spacing of the images of the two sub-eyes on the receiver of the receiving system is

$$\begin{bmatrix} d_{sv} & 0 \\ 0 & 1 \end{bmatrix}=\begin{bmatrix} \Delta\theta \cdot r_c & 0 \\ 0 & \dfrac{2y'}{D_s} \end{bmatrix} \tag{17}$$

It can be calculated according to the Eq. (17) that $d_{sv}=0.272$ mm, satisfy the requirement that the images of sub-eyes do not overlap.

3.3 Diffraction surface analysis

The diffractive surface is a phase-type optical surface, and its rotationally symmetric aspherical surface diffractive equationcan be expressed as

$$\begin{bmatrix} Z(r) & 0 \\ 0 & 1 \end{bmatrix}=\begin{bmatrix} cr^2 & -(A_4Y_4+\cdots+A_NY_N) \\ 1 & \dfrac{1}{1+\sqrt{1-(1+k)c^2r^2}} \end{bmatrix}+\begin{bmatrix} \dfrac{\lambda_0}{n(\lambda_0)-1} & \mathrm{int}\left[\dfrac{\varphi(r)'}{2\pi}\right] \\ \dfrac{\lambda_0}{n(\lambda_0)-1} & \dfrac{D_nY^2}{2\pi} \end{bmatrix} \tag{18}$$

where r is the radius of surface; Y is the ordinate; k is the conic coefficient; c is the reciprocal of the curvature; $\varphi(r)'$ is the basic formula of the diffractive surface element; the phase function $\varphi(r)'$ represents the amplitude of the surface error; A_n is the aspherical coefficient; λ_0 is the wavelength; $n(\lambda_0)$ is the refractive index; D_n is the phase coefficient. The width of the three diffractive faces of the design are 0.266 mm, 0.219 mm and 0.293 mm, and the depth of the diffractive surface is 16.706 μm. The aspect ratio satisfies the requirement of less than 1/10[11]. The phase fitting model of the diffractive surface is obtained as shown in Fig. 14, in which blue region represents the diffraction phase morphology and red region represents the complete diffractive surface morphology after superposition.

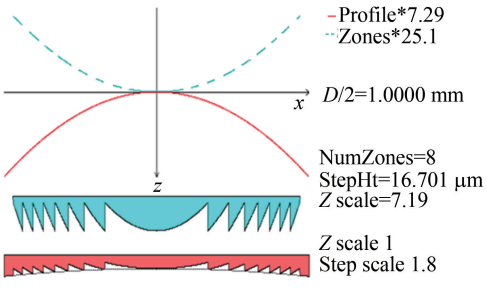

(a) Diffraction face type of the sub-eye lens

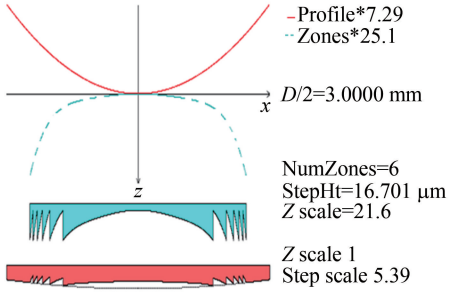

(b) Diffraction plane type of the sixth surface of the receiving system

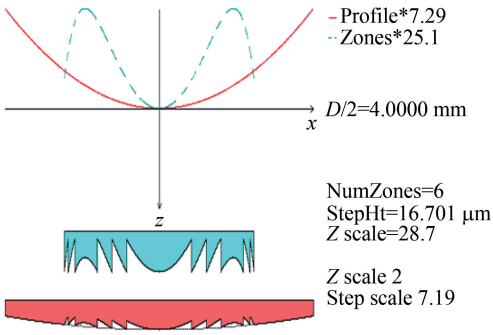

(c) Receiver system ninth diffraction surface type

Fig.14 Diffraction surface turning simulation

4 Conclusion

In this work, a visible light and long wave infrared wide spectrum compound-eye optical system is designed by theoretical derivation of the dual-band common imaging position. The system can simultaneously receive target information in the visible and long-wave infrared bands, thereby expanding the spectral receiving range of the compound eye system. In the designed sub-eye lens, the visible light band transfer function value is higher than 0.4 at the Nyquist frequency50 lp/mm, and the infrared band transfer function value reaches 0.4 at the Nyquist frequency17 lp/mm. In the designed receiving system, the value of the visible band transfer function is higher than 0.4 at the Nyquist frequency 150 lp/mm, and the value of the infrared band transfer function reaches 0.4 at the Nyquist frequency17 lp/mm. Athermalization is achieved over the temperature range $-40°\sim+60$ ℃. The results of the diffractive surface analysis prove that the system can be processed.

References

[1] MA Meng-gao, GUO Fang, CAO Zhao-lou, *et al*. Development of an artificial compound eye system for three-dimensional object detection[J]. *Applied Optics*, 2014, **53**(6): 1166-1172.

[2] SUN Hua-bo, ZHAO Hai-meng, MOONEY P, *et al*. A novel system for moving object detection using bionic compound eyes[J]. *Journal Bionic Engineering*, 2011, **8**(3): 313-322.

[3] WANG Tian, YU Wei-xing, LI Chen, *et al*. Biomimetic compound eye with a high numerical aperture and anti-reflective nanostructures on curved surfaces[J]. *Optics Letters*, 2012, **37**(12): 2397-2399.

[4] AWWAL A A S, HORISAKI R, IFTEKHARUDDIN K M, *et al*. 3D information acquisition using a compound imaging system[J]. *Optics and Photonics for Information Processing*, 2007, **6695**: 66950F.

[5] SONG Yong-min, XIE Yi-zhu, MALYARCHUK V, *et al*. Digital cameras with designs inspired by the arthropod eye [J]. *Nature*, 2013, **497**(7447): 95-99.

[6] DUNKEL J, WIPPERMANN F, REIRNANN A, *et al*. Fabrication of micro-optical freeform arrays on Wafer level for imaging applications[J]. *Optics Express*, 2015, **23**(25): 31915-25.

[7] PANG Kuo, SONG Le, FANG Feng-zhou. Large field of view curved compound eye imaging system using optical freeform surface [J]. *Journal of Optoelectronics · Laser*, 2018, **1**(29): 8-13.

[8] ZHANG Zhi-ming, GAO Yi-qing, LUO Ning-ning, *et al*. Fast fabrication of curved Micro-lens array using DMD-based lithography[J]. *AIP Advances*, 2016, **6**(1): 015319

[9] TANIDA J, SHOGENJI R, KITAMURA Y, *et al*. Color imaging with an integrated compound imaging system[J]. *Optics Express*, 2003, **11**(18): 2109-2117.

[10] DUPARRE J, DANNBERG P, SCHREIBER P, *et al*. Artificial apposition compound eye fabricated by micro-optics technology[J]. *Applied Optics*, 2004, **43**(22): 4303-4310.

[11] DUPARRE J, DANNBERG P, SCHREIBER P, *et al*. Thin compound-eye camera[J]. *Applied Optics*, 2005, **44**(15): 2949-2956.

[12] BRUCKNER A, OBERDORSTER A, DUNKEL J, *et al*. Ultra-slim 2D-and depth-imaging camera modules for mobile

imaging[C]. SPIE, 2016, **9760**: 97600N.

[13] WANG Yu-wei, CAI Bo-lin, LU Yu, *et al*. Optical system design of artificial compound eye based on field stitching[J]. *Microwave and Optical Technology Letters*, 2017, **59**(6): 1277-1279.

[14] DENG Ze-fang, CHEN Feng, YANG Qing, *et al*. Dragonfly-eye-inspired artificial compound eyes with sophisticated imaging[J]. *Advanced Functional Materials*, 2016, **26**(12): 1995-2001.

[15] ZHANG Shu-qing, ZHOU Lu-yang, XUE Chang-xi, *et al*. Design and simulation of a superposition compound eye system based on hybrid diffractive-refractive lenses[J]. *Applied Optics*, 2017, **56**(26): 7442-7449.